JOURNAL OF CATALYSIS 136, 182–196 (1992)

CO Hydrogenation over $PdNi_x$ Alloys Encaged in NaY Zeolite

JENNIFER S. FEELEY, ALEXANDER YU. STAKHEEV, FERNANDO A. P. CAVALCANTI, AND WOLFGANG M. H. SACHTLER

V. N. Ipatieff Laboratory, Center for Catalysis and Surface Science, Northwestern University, Evanston, Illinois 60208-3000

Received June 28, 1991; revised February 4, 1992

Bimetallic (Pd + Ni)/NaY samples were studied and compared with monometallic Pd/NaY and Ni/NaY samples and their physical mixture. Samples were characterized by XRD, XPS, and CO hydrogenation. The formation of $PdNi_x$ alloy particles encaged in NaY zeolite was found for the bimetallic samples. Under conditions of CO hydrogenation, significant changes in sizes and distributions of Pd, Ni, and $PdNi_x$ particles take place. Metal particle growth is accompanied by local collapse of the zeolite lattice. The selectivity of $PdNi_x$ alloys for methane formation was significantly higher than that of monometallic Pd or Ni particles or of their physical mixtures. On mixed $PdNi_x$ ensembles the rate of CO dissociation and/or CH_x hydrogenation appears to be enhanced with respect to monometallic ensembles. Acid "leaching" of Ni by zeolite protons from alloy particles restores a metal surface rich in Pd, leading to an enhanced selectivity to methanol and its consecutive products, dimethyl ether and higher hydrocarbons.

INTRODUCTION

In this study CO hydrogenation is used as a potential probe for the formation of $PdNi_x$ alloy particles. We chose these metals because in pure form they lead this reaction toward different products.

Palladium is known to catalyze the formation of methanol, in particular at high pressures, although its selectivity can be significantly modified by promotors and supports (*1–9*). Part of the support effects may be geometric in nature. Boudart and McDonald (*1*) assume that very small Pd particles containing sites of high coordinative unsaturation can dissociate CO, thus leading to methane, whereas larger particles catalyze formation of methanol via undissociated CO. Our previous data on zeolite-encaged Pd catalysts can be rationalized in terms of this model (*2, 5*) without excluding chemical or electronic interactions between Pd particles and their environment. In these studies the Pd particles inside the zeolite cavities were initially very small and methane was preferentially formed. As the reaction continued and the Pd particles grew, the selectivity for methanol, dimethyl ether (DME), and branched hydrocarbons increased significantly (*2, 5, 6*). Formation of branched molecules suggests secondary reactions of methanol and DME on Brønsted sites.

Supported nickel catalysts are well known for their high selectivity toward methane formation in CO hydrogenation (*1, 10*). Other products include linear higher hydrocarbons, which may isomerize in the presence of acid sites to form branched products. Formation of methanol, however, has not been observed on Ni. Boudart and McDonald (*1*) postulated that CO dissociation on Ni is a structure-sensitive step for the methanation reaction. Dissociative CO adsorption will be kinetically significant only under conditions where hydrogenation of adsorbed C and O atoms will be fast, i.e., at high H_2/CO ratios. Dissociative adsorption is known to be suppressed by alloying or by the presence of sulfur, i.e., when the large ensembles required for this step are in short supply.

Previous results (*11, 12*) on (Pd + Ni)/

0021-9517/92 $5.00

NaY samples have identified the conditions under which $PdNi_x$ alloy formation occurs. Significant differences in reduction and chemisorption properties were found between bimetallic samples containing alloy particles and physical mixtures of monometallic Pd/NaY and Ni/NaY. In the present work, use is made of these findings to study the activity and selectivity of NaY supported $PdNi_x$ alloys for CO hydrogenation. The alloys are compared with monometallic Pd/NaY and Ni/NaY, as well as their physical mixture. The effect on catalysis of selective leaching of Ni^0 from $PdNi_x$ alloy particles is examined (*12*). X-ray diffraction (XRD) and X-ray photoelectron spectroscopy (XPS) are used to study metal particle sizes and distribution as well as zeolite crystallinity.

EXPERIMENTAL

Sample Preparation

All samples were prepared by ion exchange for 24 h at room temperature using dilute $Ni(NO_3)_2$ and/or $Pd(NH_3)_4(NO_3)_2$ solutions. Bimetallic samples were prepared by simultaneous exchange of Ni^{2+} and $Pd(NH_3)_4^{2+}$ for Na^+ ions. The following three batches were prepared: monometallic Ni/NaY containing 8.8 Ni/unit cell, monometallic Pd/NaY containing 10.2 Pd/unit cell, and bimetallic (Pd + Ni)/NaY containing 9.1 Ni + 9.1 Pd/unit cell. Half of each batch was washed at pH 6.0 to prepare A series samples, and the other half was washed at pH 10.5 for B series samples. Details of the pH washing procedure were presented in a previous paper (*11*). The samples of the A and B series have the same Ni and Pd contents as determined by atomic absorption. The following nomenclature is used to refer to samples: Me(A or B) where Me = Ni, Pd, or PdNi and A or B refers to wash at pH 6 or 10.5, respectively, subsequent to ion exchange.

All samples were calcined in a high flow of ultrahigh-purity oxygen from 25 to 500°C with a heating ramp of 0.5°C/min and then held at 500°C for 2 h. This procedure ensures complete oxidation of the ammine ligands on Pd (*11, 13*). Samples were then stored for at least 24 h in a dessicator containing a saturated solution of NaCl in order to ensure that samples were of constant water content before weighing for reaction studies.

CO Hydrogenation

A stainless-steel Xytel high-pressure reaction system (*14*) was used for catalytic studies. Samples (ca. 250 mg) were slowly (ca. 0.5–0.7°C/min) heated to 500°C in 10.5 atm ultrahigh-purity He and then held at 500°C in He for 2 h. Reduction in all cases was carried out for 1 h at 8 atm in a 34 ml/min flow of ultrahigh-purity H_2 at 500°C after the He pretreatment. One sample, Ni(A), was reduced to 760°C *ex situ* before introduction into the Xytel reactor and then rereduced to 500°C in the reactor. After reduction, samples were cooled in H_2 flow to 300°C and then purged at 300°C for 1 h in He flow, 20 ml/min, at 10.5 atm. One bimetallic sample, which had been cooled in He instead of H_2, was also investigated in order to study the effect of Ni reoxidation, which is known to occur between 400 and 760°C. This "purged" sample will be referred to as PdNi(B)-P.

After the pretreatment described above, CO hydrogenation was carried out at 10.5 atm using a 1 : 1 mixture of $CO : H_2$ and a flow of ca. 29 ml/min. An on-line GC was used for product analysis. Data were collected at 15 min time on stream and every 30 min thereafter for 20–24 h, at which point the reaction had reached quasi-steady state. The flow rate was then halved twice to determine the effects of space velocity.

XPS

All samples were studied by XPS after CO hydrogenation. XP spectra were recorded using a VG ESCALAB-5 spectrometer using unmonochromatized Al$K\alpha$ radiation. The spectrometer was equipped with a high-pressure reaction cell to carry out sample pretreatment in various atmospheres at elevated temperature. Samples were rereduced

for 1 h in flowing hydrogen at 500°C before measurement. After this pretreatment, samples were transported to the analytical chamber of the spectrometer without contact with air. The adventitious carbon 1*s* line (285.0 eV) was used as a reference of the energy scale. The charging effect for the reduced samples was cross-checked with the binding energy of Si 2*p* line (103.5 eV) determined for a NaY blank and unreduced samples. Values of modified Auger parameter for Pd were also determined using X-ray excited M_5VV transition (*15*).

X-Ray Diffraction

Powder X-ray diffraction measurements were carried out using nickel-filtered Cu$K\alpha$ radiation at 50 kV and 25 mA, with a Rigaku Geigerflex diffractometer. Continuous X-ray scans were carried out from 2Θ of 10° to 50° with a step width of 0.02° and a counting time of 2 s.

Samples were studied after reduction and after CO hydrogenation. Reduced samples were prepared by reducing calcined samples *in situ* in a 5% H_2/Ar flow, 25 ml/min, from room temperature to 500°C at 8°C/min, and then holding at 500°C for 1 h and cooling to room temperature in the reducing atmosphere before purging in Ar for 20 min. Due to the low reducibility of Ni in the Ni(A) sample (*11*), a reduction temperature of 760°C was chosen instead of 500°C for this one sample. No attempt was made to rereduce the freshly reduced or the spent catalysts; measurements were carried out *ex situ* on air-exposed samples.

RESULTS

X-Ray Diffraction

Zeolite crystallinity. In Table 1 the ratios of the relative X-ray diffraction peak intensities before and after reaction are presented. The XRD peak positions for NaY, which are least sensitive to zeolite water content (*16*) and 2Θ values of 20.3, 23.6, and 27.0 corresponding to the Miller indices (440), (533), and (642), respectively, were used to estimate zeolite crystallinity. From reproducibility studies the experimental error in X-ray measurements is estimated to be ±5%. Previous studies on similar samples (*11*) showed no loss in crystallinity upon ion exchange, pH wash, and calcination to 500°C. Of the samples studied in this work after reduction, only Ni(A), which had been reduced to 760°C, showed an appreciable loss in crystallinity. For this sample a loss of ca. 30% in zeolite crystallinity was detected after the reduction step. All other samples showed no significant framework breakdown after reduction.

TABLE 1

X-Ray Diffraction Results: Crystallinity

Sample	X-ray intensity ratio,[a] Spent/reduced		
	440	533	642
Ni(A)	0.97	1.01	1.00
Ni(B)	0.71	0.81	0.74
Pd(A)	1.00	0.96	1.03
Pd(B)	0.96	0.78	0.97
PdNi(A)	0.85	0.83	0.69
PdNi(B)	0.91	0.91	1.05
NaY–H_2O/NaY[b]	0.93	1.03	0.99
PdNi(B)–CO[c]	0.89	1.05	0.92

[a] Ratios of peak intensities for samples after CO hydrogenation during 24 h/freshly reduced samples.

[b] Ratios of peak intensities for NaY blank after exposure to 0.5 atm H_2O for 24 h at 300°C/NaY.

[c] Ratios of peak intensities for PdNi(B) after reduction to 500°C and exposure to CO at 60°C for 48 h/PdNi(B) after reduction to 500°C.

Loss in crystallinity, ≤30%, was observed for some samples after CO hydrogenation. In order to separate effects of particle growth and steam on framework breakdown, a NaY blank sample was studied after exposure to 0.5 atm H_2O at 300°C for 24 h. Calculations from reaction conversion data indicated that this partial pressure of H_2O was approximately equal to the amount of water present under the highest conversion conditions studied. Comparison of the XRD profiles of NaY with this steam-

TABLE 2

X-Ray Diffraction Results: Particle Size

Sample	After reduction[a]	After reaction[b]
Ni(A)	23.3 nm	12.6 nm
Ni(B)	<3.0 nm	23.9 nm
Pd(A)	<3.0 nm	<3.0 nm
Pd(B)	<3.0 nm	6.5 nm
PdNi(A)	<3.0 nm	6.6 nm
PdNi(B)	7.6 nm	7.1 nm

[a] All samples, except for Ni(A), which was reduced to 760°C, were reduced to 500°C.

[b] After CO hydrogenation as described under Experimental.

treated sample showed no significant loss in crystallinity. In addition for all samples showing a loss of crystallinity in Table 1, a corresponding growth in metal particle size during reaction was found (Table 2). We therefore assume that the growth of metal particles is the major cause of local collapse of the zeolite framework.

Ni/NaY samples. The XRD profiles of the monometallic Ni/NaY samples are presented in Fig. 1. In Table 2 the average Ni particle sizes are summarized for samples after reduction and after reaction. These average Ni particle sizes were calculated with the Scherrer equation (*17*) by analysis of the Ni(111) peak at $2\Theta = 44.627°$ (lattice constant 3.5168 Å) (*18*). As mentioned, large particles of ca. 23.3 nm, Fig. 1a, are seen after reduction for Ni(A). After reaction the intensity of the Ni(111) peak has decreased significantly, as trace (b) in Fig. 1 shows; the average particle size appears to be ca. 12.6 nm. Some error in these numbers is due to the presence of a zeolite XRD peak at ca 44.5°C. For Ni(B) the opposite trend is observed: the average Ni particle size increases dramatically during reaction, i.e., from <3 to 23.9 nm.

Pd/NaY samples. In Fig. 2 and Table 2, results are presented for monometallic Pd samples. The Scherrer formula was used for average Pd particle size determinations for analysis of the Pd(111) peak at $2\Theta = 40.228$ (lattice constant 3.8827 Å) (*18*). A similar trend, as seen for the monometallic Ni samples, is found for the monometallic Pd samples. The A series sample shows less particle growth during reaction than the B series sample. After reduction of Pd(A), a broad peak characteristic of small Pd particles, <3 nm, is observed. After reaction, a small

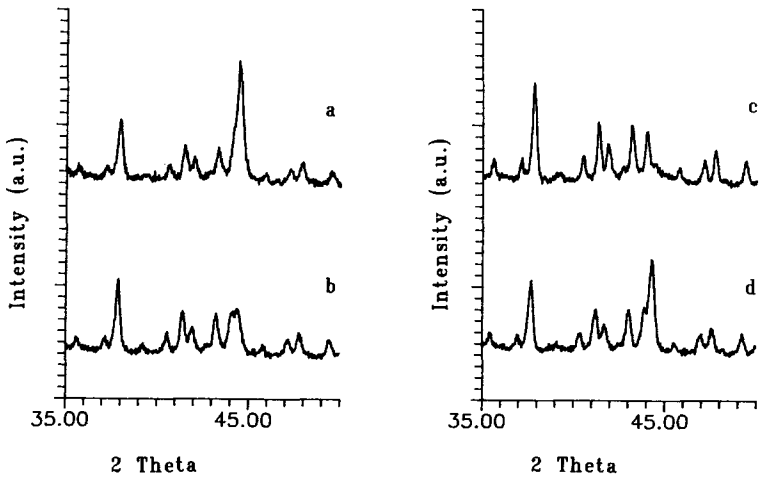

FIG. 1. XRD profiles of: (a) Ni(A) after reduction; (b) Ni(A) after CO hydrogenation; (c) Ni(B) after reduction; (d) Ni(B) after CO hydrogenation.

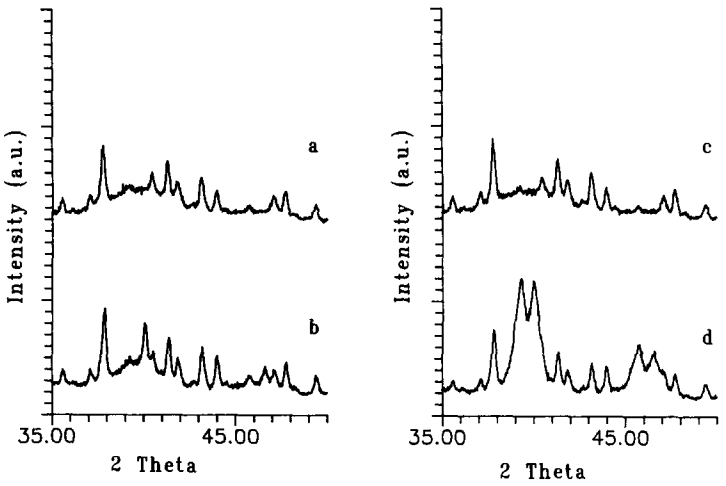

FIG. 2. XRD profiles of: (a) Pd(A) after reduction; (b) Pd(A) after CO hydrogenation; (c) Pd(B) after reduction; (d) Pd(B) after CO hydrogenation.

Pd(111) peak is present; however, the average particle size cannot be accurately determined with XRD indicating that the majority of particles are less than ca. 3 nm. For Pd(B) the XRD profile before reaction (Fig. 2c) is virtually identical to that of Pd(A) before reaction (Fig. 2a); however, after reaction of Pd(B) (Fig. 2d), large Pd particles (ca. 6.5 nm) are observed. In addition a peak at 2Θ of ca. 39.1°, which is thought to be due to palladium interstitial with carbon (*6*), is observed. This peak was found absent in samples that were reduced in H_2 after reaction to remove carbon.

Bimetallic (Pd + Ni)/NaY samples. The XRD profiles for the bimetallic samples before and after reaction are presented in Fig. 3. For bimetallic catalysts with a wide distribution of compositions of the individual particles, the line width does not reflect particle size. Being aware of this we present the "particle sizes" calculated from Scherrer's

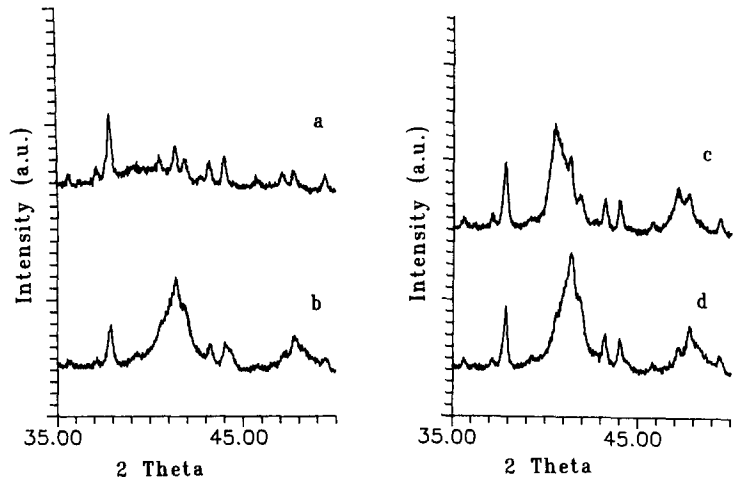

FIG. 3. XRD profiles of: (a) PdNi(A) after reduction; (b) PdNi(A) after CO hydrogenation; (c) PdNi(B) after reduction; (d) PdNi(B) after CO hydrogenation.

formula, Table 2, as purely empirical parameters that are only very roughly related to the true particle sizes.

During reaction, the particle size for the bimetallic PdNi(A) sample increases from <3 to ca. 6.6 nm. The average particle size of the bimetallic PdNi(B) samples appears to be about the same before and after reaction, i.e., ca. 7.1–7.6 nm; however, the position of the X-ray peak shifts to a lower average lattice constant, i.e., higher 2Θ, during reaction. The two bimetallic samples (Figs. 3b and 3d) had very similar XRD profiles after reaction. Qualitative estimates using Végard's law (*18*) indicate that the large $PdNi_x$ particles probed with XRD after reaction are somewhat richer in Pd (average mole percent Pd ca. 70%) than the overall 1 : 1 composition confirmed by chemical analysis. However, the peaks are very broad indicating a large distribution of particle compositions. It is significant that in contrast to the monometallic samples, no isolated monometallic Pd or Ni particles >3 nm are detected in any of the bimetallic samples (Fig. 3).

XPS Results

XPS atomic ratios and binding energies are summarized in Tables 3 and 4, respectively, for monometallic and bimetallic samples after CO hydrogenation. The experimental error in atomic ratios is estimated to be ±10% and in binding energies ±0.1 eV

TABLE 3

XPS Atomic Ratios

Sample	Pd/Si	Ni/Si	Pd/Ni	Al/Si	O/Si
Ni(A)	—	0.014	—	0.26	3.05
Ni(B)	—	0.034	—	0.26	2.99
Bulk	—	0.065	—	0.41	2.82
Pd(A)	0.019	—	—	0.23	3.02
Pd(B)	0.032	—	—	0.22	3.06
Bulk	0.075	—	—	0.41	2.82
PdNi(A)	0.015	0.010	1.53	0.28	2.94
PdNi(B)	0.028	0.023	1.25	0.25	3.15
Bulk	0.067	0.067	1.0	0.41	2.82

TABLE 4

XPS Binding Energies

Sample	Pd 3*d*	AP[a] Pd	Ni 2*p*	Si 2*p*	Al 2*p*	O 1*s*
Ni(A)	—	—	851.4	103.5	75.3	532.2
Ni(B)	—	—	851.3	103.5	75.6	532.3
Pd(A)	335.4	664.6	—	103.5	75.3	532.4
Pd(B)	335.0	663.8	—	103.5	75.2	532.3
PdNi(A)	334.7	663.6	851.1	103.5	75.5	532.4
PdNi(B)	334.7	663.5	851.3	103.5	75.4	532.3

[a] AP, Auger parameter.

(*15*). "Bulk" metal/Si ratios were calculated from chemical analysis of the samples.

Monometallic Ni samples. After CO hydrogenation, the Ni $2p_{3/2}$ binding energies, 851.3 and 851.4 eV for Ni(B) and Ni(A), respectively, indicate that Ni is overwhelmingly in the metallic state in both catalysts (*19*). No nickel carbide is detected by XPS. Even if Ni carbide is formed during the catalytic reaction, it will be destroyed during the H_2 treatment prior to XPS data collection. The Ni/Si ratios, 0.034 and 0.014 for Ni(B) and Ni(A), respectively, are significantly lower than the overall bulk ratio of 0.065. Considering the high sensitivity of XPS for metal agglomeration at the external surface of the zeolite (*20*), these data suggest that such migration is not significant under reaction conditions.

Monometallic Pd samples. XPS data show that under reaction conditions, the structure of Pd(B) differs significantly from that of Pd(A). For Pd(B) the binding energy of the Pd $3d_{5/2}$ line, 335.0 eV, and the Pd Auger parameter, 663.8 eV, are close to the values of bulk Pd metal, 335.0 and 663.7 eV, respectively, indicating the presence of large Pd particles under reaction conditions (*15*). XPS data indicate that these particles are predominantly located in the interior of zeolite crystallites; the Pd/Si ratio, 0.032, for this sample is less than the bulk value, 0.075. For Pd(A), the binding energy of the Pd $3d_{5/2}$ line, 335.4, is significantly higher than that of bulk Pd. This difference can be attributed to the formation of very small

metal clusters that are electron deficient due to electron transfer between these clusters and zeolite acid sites (*15*). The value of the Pd(A) Auger parameter, 664.6 eV, is somewhat higher than that of the bulk metal. The Pd/Si ratio, 0.019, for Pd(A) is lower than the bulk value indicating that the majority of Pd particles are located in the interior of zeolite crystallites.

Bimetallic (Pd + Ni)/NaY samples. After their use in CO hydrogenation the structures of PdNi(A) and PdNi(B) are very similar. Their Pd/Ni ratios are 1.53 and 1.25 for PdNi(A) and PdNi(B), respectively, indicating an enrichment of Pd in the particles near the surface that are probed with XPS. In both samples, the Pd $3d_{5/2}$ and Ni $2p_{3/2}$ lines are at values characteristic of bulk metal and the values of the Ni/Si and Pd/Si atomic ratios are significantly below the overall ratios. These results indicate the presence of large particles predominantly in voids of the zeolite.

XPS data also give some evidence for alloy formation in both PdNi(A) and PdNi(B) after reaction. Unfortunately, essential shifts of Pd $3d_{5/2}$ and Ni $2p_{3/2}$ lines, due to differential charging and size effects, prevent us from giving absolute values of Pd and Ni binding energies as functions of alloy composition. However, as charging will lead to an equal shift for Ni $2p_{3/2}$ and Pd $3d_{5/2}$ lines in a given particle, the distance between these lines is insensitive to differential charging. For the pure metals, Hillebrecht *et al.* (*21*) calculated the distance between these two lines to be 517.45 eV versus 516.8 eV for a $Pd_{0.5}Ni_{0.5}$ alloy. Using the data in Table 4, one can calculate that this distance is equal to 516.4 eV after reaction for PdNi(A) and 516.6 eV for PdNi(B). These results indicate the presence of $PdNi_x$ alloy particles in both cases.

Another parameter sensitive to alloy formation is the distance between the Ni $2p_{3/2}$ main line and the core hole satellite. Steiner and Hüfner (*22*) showed that increasing the Pd concentration in a $PdNi_x$ alloy causes a shift of the satellite peak in the Ni $2p_{3/2}$ spectrum closer to the main line. Figure 4 shows this shift for PdNi(B) compared to Ni(B), providing additional evidence for alloy formation in our bimetallic catalysts. Similar results were found for PdNi(A).

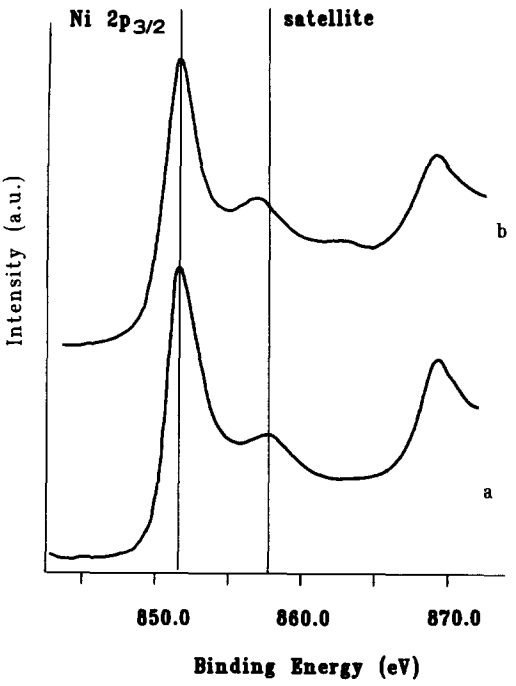

FIG. 4. XPS spectra after CO hydrogenation: (a) Ni(B); (b) PdNi(B).

CO Hydrogenation

General results. All reaction runs were repeated at least twice; results were reproducible within 10%. Chemical analysis for all samples before and after reaction showed no loss of metal. Carbon molar selectivities (Table 5) are defined as the amount of carbon in each product divided by the total amount of carbon converted from CO to hydrocarbons and oxygenates excluding CO_2.

The conversion results presented in Table 5 are normalized to the total amount of metal in the catalysts. This method was used because of the XRD and XPS findings that indicated that Pd, Ni, and $PdNi_x$ particle sizes change during the course of CO hydrogenation.

TABLE 5

Summary of Steady-State CO Hydrogenation Results

Sample	C Molar Selectivities										
	C_1	C_2	C_3	C_4	C_5	C_6	C_7	CH_3OH	DME	$i/(i+n)$[a]	CO_{conv}[b]
Pd(A)	63.0	2.9	0.1	—	—	—	—	12.0	22.0	—	15.64
Pd(B)	43.0	8.1	11.3	21.0	8.1	4.3	1.1	2.5	0.7	0.73	4.29
Ni(A)	73.0	15.9	6.5	3.2	1.1	0.3	—	—	—	0.55	2.55
Ni(B)	79.0	10.3	6.3	2.5	1.3	0.6	—	—	—	0.49	7.22
PdNi(A)	92.0	2.1	0.7	0.5	0.2	—	—	3.1	1.4	0.55	10.94
PdNi(B) mix	91.2	2.5	1.0	0.3	0.5	—	—	3.5	1.0	0.52	11.89
PdNi(B)–P	73.0	4.2	3.8	5.8	3.2	2.2	0.8	5.0	2.0	0.66	6.40
$PdNi_{mix}$	64.0	9.8	6.1	9.7	4.7	2.7	0.7	2.0	0.3	0.71	5.26
W. Ave[c]	63.5	12.0	9.1	8.5	3.5	1.8	0.4	1.0	0.2	0.61	4.64

[a] iso: (iso + normal) C_4 ratio.
[b] No. CO_{conv}/No. (Pd + Ni)/$s \times 10^{-4}$.
[c] Weighted average of results for Pd(B) and Ni(B) samples.

Decreasing the space velocity, from ca. 900 to 200 h^{-1}, had little effect on the selectivities of the catalysts, the methane selectivities increased <10%. The conversions of all catalysts varied approximately linearly with space velocity, increasing with decreasing space velocity.

Monometallic Pd/NaY. The carbon molar selectivities after 20 h for the two monometallic Pd samples are summarized in Table 5. Figures 5a and 5b display the normalized yields over Pd(A) and Pd(B) respectively as a function of time on stream (TOS). The carbon production for each reaction product is normalized to the initial methane production at 15 min TOS (Pd(A), 2.52×10^{-3} μmol CH_4/μmol Pd/s; Pd(B), 1.35×10^{-3} μmol CH_4/μmol Pd/s). Comparison of Figs. 5a and 5b shows that activities and selectivities of these catalysts are very different. Both catalysts seem to be active for methanol and DME formation. On Pd(A) secondary reactions to higher hydrocarbons are small; propane is the highest hydrocarbon detected and it accounts for less than 0.5% of the total carbon. In contrast on Pd(B), the production of higher hydrocarbons is high. Its distribution does not follow the Anderson–Schulz–Flory distribution. Also, for Pd(B), the iso/(iso + normal) C_4 ratio is higher than the equilibrium value of 0.5. The activity normalized to the total amount of Pd in the sample is ca. 3.5 times higher for Pd(A) than for Pd(B), and the methane selectivity is higher over Pd(A).

Monometallic Ni/NaY. The results on these two samples are shown in Table 5. The product formation as a function of TOS for Ni(B) is given in Fig. 6, where the carbon production for each product is normalized to the amount of CH_4 produced at 15 min TOS (1.024×10^{-3} μmol CH_4/μmol Ni/s). Nickel reduction is known to be 100% complete for Ni(B), and 90–95% complete for Ni(A) (*11*). The selectivities of the two Ni catalysts in CO hydrogenation are quite similar; therefore no figure is given for Ni(A). Both catalysts form mainly methane. After 20 h on stream the activity is 2.8 times higher for Ni(A) than for Ni(B). The ratios of iso/(iso + normal) C_4's, 0.55 and 0.49 for Ni(A) and Ni(B), respectively, are close to the equilibrium value of 0.50.

Bimetallic (Pd + Ni)/NaY. Figure 7 shows the reaction results for PdNi(B) as a function of reaction time, with the carbon production for each product normalized to the amount of CH_4 produced at 15 min TOS

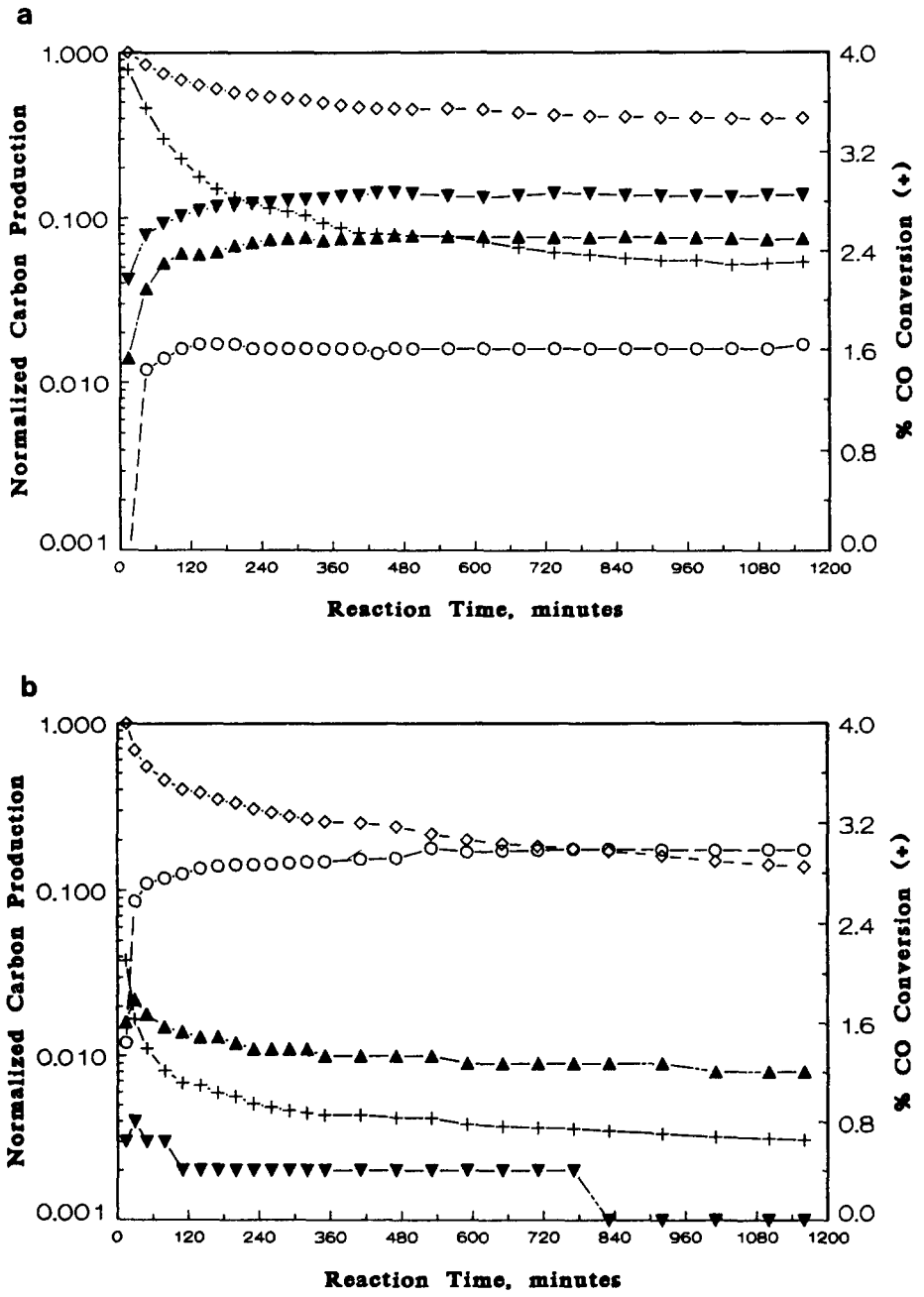

FIG. 5. CO hydrogenation results for (a) Pd(A), CO : H_2 = 1 : 1, P = 10.5 atm, T (reaction temperature) = 295°C, GHSV 903; (b) Pd(B), CO : H_2 = 1 : 1, P = 10.5 atm, T = 295°C, GHSV = 864. (◇) CH_4; (○) C_{2+} hydrocarbon; (▲) CH_3OH; (▼) CH_3OCH_3; (+) % CO conversion.

(1.21×10^{-2} μmol CH_4/μmol (Pd + Ni)/s). The behavior of PdNi(A) is very similar; its results are presented in Table 5. Both bimetallic samples exhibit high selectivity for methane formation. In fact, the yields (based on CO conversion) and the selectivity for methane are higher over the bimetallic samples than over monometallic Ni. Additional products include small amounts of methanol, DME, and higher hydrocarbons.

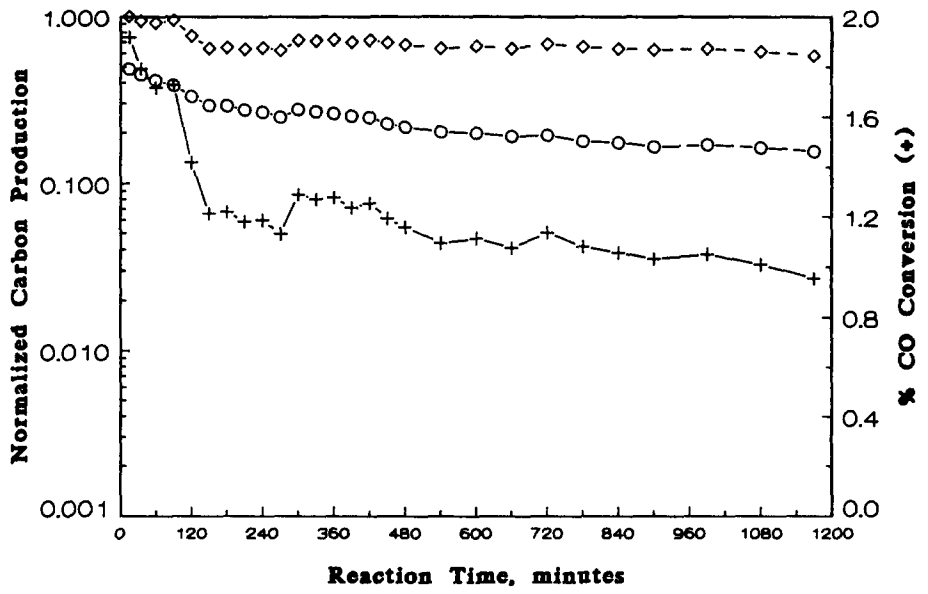

FIG. 6. CO hydrogenation results for Ni(B). CO : H_2 = 1 : 1, P = 10.5 atm, T = 295°C, GHSV = 899. (◇) CH_4; (○) C_{2+} hydrocarbon; (▲) CH_3OH; (▼) CH_3OCH_3; (+) % CO conversion.

These bimetallic catalysts deactivate more rapidly than monometallic samples. The iso/(iso + normal) C_4 ratio is close to the equilibrium value, similar to findings for the monometallic Ni samples, and in contrast to results for the monometallic Pd(B) sample.

Physical mixture and purged bimetallic sample. The quasi-steady-state results for a physical mixture of Ni(B) and Pd(B), referred to as $PdNi(B)_{mix}$, are presented in Table 5, along with the values calculated for the weighted average, W.Ave, of the

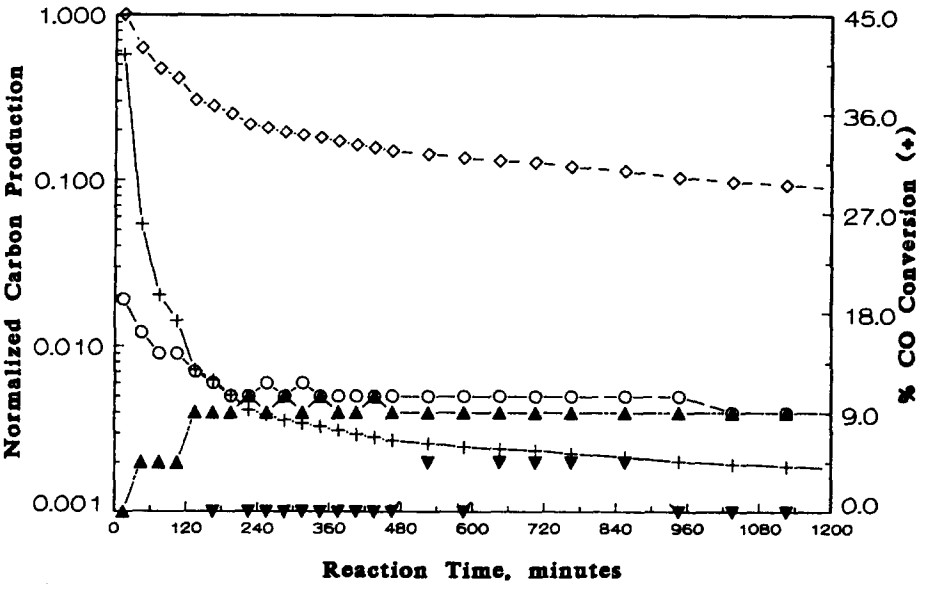

FIG. 7. CO hydrogenation results for PdNi(B). CO : H_2 = 1 : 1, P = 10.5 atm, T = 295°C, GHSV = 700. (◇) CH_4; (○) C_{2+} hydrocarbon; (▲) CH_3OH; (▼) CH_3OCH_3; (+) % CO conversion.

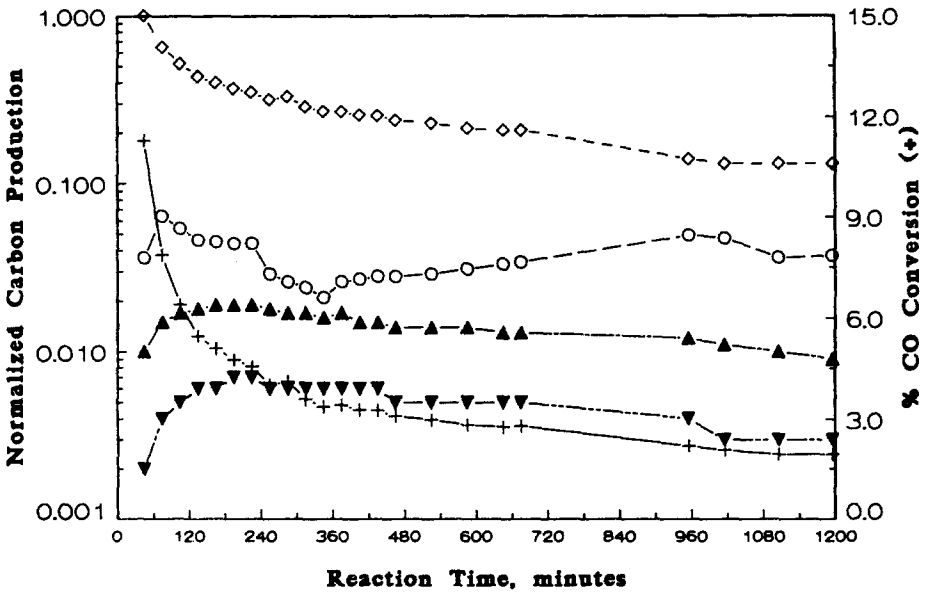

FIG. 8. CO hydrogenation results for PdNi(B)–P. CO : H_2 = 1 : 1, P = 10.5 atm, T = 295°C, GHSV = 776. (◇) CH_4; (○) C_{2+} hydrocarbon; (▲) CH_3OH; (▼) CH_3OCH_3; (+) % CO conversion.

monometallic samples. Within experimental error, the physical mixture has an activity and selectivity equal to the linear combination of the monometallic samples comprising the mixture. The high activity and selectivity for methanation found for the bimetallic samples are not observed on the physical mixture.

The purged bimetallic sample, PdNi(B)-P, which was treated in an identical manner except that it was cooled from 500 to 300°C in He instead of in H_2,markedly differs from the bimetallic sample PdNi(B); see Fig. 8 and Table 5. In Fig. 8, the carbon production for each product is normalized to the initial CH_4 production at 15 min TOS, which was 3.55×10^{-3} μmol CH_4/μmol (Pd + Ni)/s. In comparison to the "normal" bimetallic PdNi(B) sample, the purged sample shows a much lower selectivity and activity for methane formation; the selectivity toward higher hydrocarbons, methanol, and DME on the other hand increases, and the iso/(iso + normal) C_4 ratio is higher, exceeding the equilibrium value. This product pattern is similar to that of monometallic Pd(B).

DISCUSSION

Changes in catalytic activity and selectivity with time on stream are accompanied by significant changes of metal particle sizes, locations, and alloy compositions. The catalysts behave as dynamic systems revealing significant mobility of metal atoms under the conditions of the catalytic process. As a result it is not possible to give meaningful numbers for the turnover frequencies. As reported in (*12*), we measured the chemisorption of hydrogen on the fresh catalysts by TPD; if one uses these data as a basis for a rough estimate of the TOF, ignoring the changes in the number of surface exposed atoms during the reaction, values between 6×10^{-4} s^{-1} for Pd(B) and 5×10^{-3} s^{-1} for Ni(B) are calculated. Values of the same order of magnitude are obtained if the metal particle sizes are estimated from the XRD line width data.

Although the misconception is widespread that zeolites are absolutely rigid and that zeolite-supported metal particles can, therefore, become larger than zeolite cages only by migrating to the external surface, the

electron microscopic observations of Bergeret and Gallezot (*23*) show that grape-shaped metal paticles extending over several contiguous supercages can be formed inside the zeolite. The present data further indicate that metal particle growth at elevated temperature can lead to local collapse of the zeolite lattice, resulting in detectable loss of zeolite crystallinity. The location of fairly large PdNi, PdCu, or PtCu alloy particles inside the zeolite also follows from the fact that zeolite protons are able to chemically interact with them, selectively "leaching" virtually all Ni or Cu atoms out of the alloy particles, as has been extensively described elsewhere (*12, 24, 25*). An analysis of particle growth versus metal migration to and from the external surface, based on the comparison of XRD and XPS results on monometallic and bimetallic samples after reduction versus after reaction, will be given in a forthcoming paper. These results provide further evidence for the presence of large metal particles inside the zeolite pore system after CO hydrogenation.

Monometallic Samples

The two monometallic Ni/NaY samples have comparable selectivity and activity profiles; both form methane predominately. The activity of zeolite-supported Ni catalysts has been reported to be lower than that of Ni/Al_2O_3 (*26, 27*). Vannice studied CO hydrogenation over Ni/SiO_2 (*28*) and Ni/Al_2O_3 (*29*) catalysts. They reported high methane selectivities and turnover frequencies (N_{CH_4}) ranging from $11–55 \times 10^{-3}$ s^{-1}. Bhatia *et al.* (*26*) found a lower N_{CH_4} for Ni/CaY ($1–7.7 \times 10^{-3}$ s^{-1}) than for Ni/Al_2O_3 ($5.6–46 \times 10^{-3}$ s^{-1}) samples. In agreement with these results, Elliot and Lunsford (*27*) found N_{CH_4} values for Ni/NaY (5×10^{-3} s^{-1}) to be lower than values for comparable Ni/Al_2O_3 (230×10^{-3} s^{-1}) samples. Our activity results are fairly similar to those reported for Y zeolite-supported Ni samples. Based on particle sizes calculated from XRD data after reaction, approximate N_{CH_4} values of 2.9×10^{-3} s^{-1} and 16.8×10^{-3} s^{-1} are calculated for the Ni(A) and Ni(B) samples, respectively. Before reaction, Ni(A), which was reduced to high temperature, 760°C, has a larger average Ni particle size by XRD than Ni(B), which was reduced at lower temperature. However, during the course of the reaction this particle size difference is apparently reversed. Growth of Ni particles in Y zeolites during CO hydrogenation was also observed by Bhatia *et al.* (*26*) and by Elliot and Lunsford (*27*).

Whereas Pd(A) and Pd(B) initially, before reaction, have similar particle sizes, i.e., <3 nm, their selectivities are quite different; Pd(A) produces primarily methane, methanol, and DME, whereas Pd(B) forms significant amounts of higher hydrocarbons. During reaction, some paticle growth is observed in Pd(A), but the majority of particles are <3 nm. In contrast, extensive particle growth is observed in Pd(B) during reaction; the average Pd particle size is ca. 6.5 nm. Our XRD and XPS results indicate that for both samples the majority of Pd particles are located in the interior of the zeolite pore system. This difference in particle size after reaction correlates with a slightly higher methane selectivity of Pd(A) versus Pd(B). For Pd/SiO_2, Ichikawa *et al.* (*4*) and Boudart and McDonald (*1*) concluded that small Pd particles are more active for methane formation than larger Pd particles, although results by Rieck and Bell (*30*) indicate the opposite trend. A comparison of the present results with those reported by others in terms of turnover frequencies is not meaningful due to the changes in particle morphology during reaction. The present results on conversion levels, selectivities, and particle sizes are, however, in agreement with previous data on samples supported on NaY and NaHY (*5, 39*).

The main difference in the catalytic behavior of the two Pd catalysts of the present study is in their selectivities to higher hydrocarbons. Only on Pd(B) is the secondary reaction of methanol and DME to form higher hydrocarbons significant. Recent results (*2*) on physical mixtures of neutralized

Pd/NaY and HY, under the same conditions as used in this study, have shown that the conversion of methanol and DME to higher hydrocarbons can take place on acid sites that can be located at some distance from Pd particles. On neutralized Pd/NaY, no secondary reactions of methanol and DME to higher hydrocarbons take place. Evidently protons are responsible for the conversion of methanol and DME to higher hydrocarbons. The catalytic data thus suggest that in the present Pd(A) catalyst, surprisingly few protons are present. It thus seems that during catalyst reduction to 500°C, dehydroxylation is more extensive for Pd(A) than for Pd(B). Evidence that dehydroxylation might be responsible for the current findings also emerges in previous studies (*2*) on the effect of reduction temperature on catalysis of a similar Pd(A) sample. Those results indicated that reduction to 350°C results in a catalyst active for the formation of higher hydrocarbons; whereas after reduction to 500°C, the selectivity is switched to methane, methanol, and DME.

Higher hydrocarbon formation on Pd-zeolite systems, as found on Pd(B), has been reported in a number of papers (*2, 5, 31, 32*). On zeolite supports, Brønsted acid sites can be formed during Pd reduction and/or be part of the original framework. These protons can react with methanol and DME to produce higher hydrocarbons via the Mobil process for the conversion of methanol to high octane gasoline (MTG process). Fujimoto *et al.* (*32*) reported on the synthesis of hydrocarbons, via production of methanol followed by the MTG process, using mixtures of Pd/SiO_2 and zeolites H-ZSM-5, HY, and H-mordenite. Thomson and Wolf (*31*) proposed the same bifunctional route for the synthesis of higher hydrocarbons over Pd/ZSM-5 catalysts. The current results are in good agreement with those recently reported for Pd/NaY catalysts (*2, 5*), but they are at variance with earlier results (*8*) on Pd/NaY and Pd/HY catalysts, where 98% methane selectivity was reported under reaction conditions very similar to those used here (280°C, 15 atm, $H_2/CO = 2.8$, GHSV = 1200 h^{-1}). We can only speculate that significant differences in catalyst precursors, calcination, and reduction conditions may be responsible for this discrepancy.

Bimetallic Samples

This paper focuses on the comparison of bimetallic NaY-supported samples with their monometallic counterparts and their physical mixture. The results show that the bimetallic samples containing mixed $PdNi_x$ alloy particles display methane selectivities much higher than those of either Pd or Ni and much lower selectivities to methanol, DME, and higher hydrocarbons. From previous results (*11, 12*) it is known that alloy formation does not occur upon reduction of physical mixtures; only isolated Pd and Ni particles are formed. The different catalytic behavior of the bimetallic catalysts, versus the physical mixture, therefore gives further evidence for the formation of alloy particles.

To our knowledge, this is the first work to report on the CO hydrogenation activity of encaged $PdNi_x$ particles in Y zeolites. Our PdNi(A) and PdNi(B) catalysts had very similar structures after reaction as probed by XRD and XPS. As would be expected from these results, they also displayed similar activities and selectivities for CO hydrogenation. Both formed methane with high selectivity and approximately the same conversions (Table 5). These results are in qualitative agreement with reported observations in the literature for $PdNi_x$ alloys supported on alumina (*33*), bulk alloys (*34*), and alloy films (*35, 36*). Working at much higher space velocities and lower pressures but similar temperatures, Bartholomew and Barton (*33*) reported a selectivity to methane of 92% for a $PdNi_x$ alloy supported on alumina at 250°C, 3.4 atm, and a GHSV of 60,000 h^{-1}. For our samples, we found 92% selectivity for methane. A high selectivity of $PdNi_x$ alloys for methane formation has been reported by other authors as well. van Barneveld and Ponec (*34*) found that methane was formed with ca. 95% selectivity

over bulk $Pd_{0.5}Ni_{0.5}$ alloys in comparison to a 65% selectivity for bulk Ni. Studies on alloy films (*35, 36*) showed a $PdNi_x$ surface to be more active and selective for methane formation than the same surface after coating with Ni.

The lower selectivity for methanol and its consecutive products of $PdNi_x$ particles, as compared to Pd particles, can be explained by the dilution of Pd ensembles with Ni atoms. Zeolite protons can reoxidize Ni atoms in $PdNi_x$ particles creating Ni^{2+} ions that escape to small zeolite cages (*12*). This "leaching" of Ni atoms out of $PdNi_x$ particles should result in an increased concentration of surface Pd atoms and a concomitant increase in selectivity for methanol and methanol-derived products. This interpretation is confirmed by the behavior of the purged sample, PdNi(B)-P. When Ni atoms are leached out of bimetallic $PdNi_x$ particles, pure Pd ensembles are recreated and the formation of methanol, DME, and higher hydrocarbons increases dramatically. In addition the iso/normal C_4 ratio, which gives an indication of the extent of formation of higher hydrocarbons via methanol and DME, increases after leaching to a value above the thermodynamic value.

IR data show that CO forms predominantly a bridging complex on Pd; i.e., chemical bonds are formed with two or three surface atoms. Assuming that the same adsorption mode is also preferred on the surface of a $PdNi_x$ alloy particle, it follows that a significant fraction of the adsorbed CO molecules will be held on a "mixed ensemble" comprising both Ni and Pd atoms. On such a site, adsorption of CO is likely to be somewhat weaker than on Ni, but stronger than on Pd ensembles of the same size. This will have consequences on the activation energies for the adsorption, the dissociation of CO, and the subsequent reaction of the adsorbed C atom with hydrogen. The situation is reminiscent of the chemistry and kinetics of hydrocarbon adsorption and hydrogenolysis on mixed ensembles on the surface of PtRe particles, which was previously studied in considerable detail (*37, 38*). In both cases, the net effect is that the cleavage reaction (i.e., CH_4 formation from $CO + H_2$ or hydrogenolysis of hydrocarbons) is kinetically preferred on mixed ensembles. We therefore propose that the enhanced selectivity for methane and the decreased selectivity for methanol and its secondary products is characteristic for the presence of mixed PdNi ensembles at the surface of the $PdNi_x$ alloy particles.

CONCLUSIONS

CO hydrogenation appears to be a good probe for $PdNi_x$ alloy formation. Physical characterization techniques give evidence for zeolite-encaged $PdNi_x$ alloys. These $PdNi_x$ alloy particles are selective methanation catalysts in comparison with physical mixtures of monometallic catalysts. During catalytic use, metal particle sizes and locations change. In addition, zeolite protons can selectively oxidize Ni atoms out of $PdNi_x$ particles to form Ni^{2+} ions. This leaching process modifies the catalytic selectivity toward that characteristic of monometallic Pd/NaY.

ACKNOWLEDGMENT

We gratefully acknowledge support from the U.S. Department of Energy, Grant DE-FGO2-87ERA13654.

REFERENCES

1. Boudart, M., and McDonald, M. A., *J. Phys. Chem.* **88,** 2185 (1984).
2. Cavalcanti, F. A. P., Dossi, C., Sheu, L.-L., and Sachtler, W. M. H., *Catal. Lett.* **6,** 289 (1990).
3. Wang, S. Y., Moon, S. H., and Vannice, M. A., *J. Catal.* **71,** 167 (1981).
4. Ichikawa, S., Poppa, H., and Boudart, M., *in* "Catalytic Materials Relationship between Structure and Reactivity" (T. E. Whyte, R. A. D. Betta, E. G. Derouane, and R. T. K. Baker, Eds.), ACS Symposium Series, p. 439. American Chemical Society, Washington, DC, 1984.
5. Sachtler, W. M. H., Cavalcanti, F. A. P., and Zhang, Z., *Catal. Lett.* **9,** 261, (1991).
6. Ziemecki, S. B., Jones, G. A., and Swartzfager, D. G., *J. Less-Common Met.* **131,** 157 (1987).
7. Poutsma, M. L., Elek, L. F., Ibarbia, P. A., Risch, A. P., and Rabo, J. A., *J. Catal.* **52,** 157 (1978).

8. Fajula, F., Anthony, R. G., and Lunsford, J. H., *J. Catal.* **73,** 237 (1982).
9. Berlowitz, P. S., and Goodman, D. W., *J. Catal.* **108,** 364 (1987).
10. Biloen, P., and Sachtler, W. M. H., *in* "Advances in Catalysis" (D. D. Eley, H. Pines, and P. B. Weisz, Eds.), Vol. 30, p. 165. Academic Press, San Diego, 1981.
11. Feeley, J. S., and Sachtler, W. M. H., *Zeolites* **10,** 738 (1990).
12. Feeley, J. S., and Sachtler, W. M. H., *J. Catal.***131,** 573 (1991).
13. Homeyer, S. T., and Sachtler, W. M. H., *J. Catal.***117,** 91 (1989).
14. Tsang, C. M., Ph.D. thesis, Northwestern University, 1988.
15. Stakheev, A. Y., and Sachtler, W. M. H., *J. Chem. Soc. Faraday Trans. 1,* **87**(22), 3703 (1991).
16. Bolton, A. P., *in* "Experimental Methods in Catalytic Research: Preparation and Examination of Practical Catalysts" (R. B. Anderson and P. T. Dawson, Eds.), Physical Chemistry: A Series of Monographs Vol. 2, pp. 1–10. Academic Press, New York, 1976.
17. Rohrbaugh, W. J., *in* "Characterization and Catalyst Development: An Interactive Approach" (S. A. Bradley, M. J. Gattuso, and R. J. Bertolacini, Eds.), ACS Symposium Series, Vol. 411, p. 279. American Chemical Society, Washington, DC, 1989.
18. Hultgren, R., and Zapffe, C. A., *Am. Inst. Mining Met. Engrs.* **58,** 1047 (1939).
19. Contarini, S., Michalik, J., Narayana, M., and Kevan, L., *J. Phys. Chem.* **90,** 4586 (1986).
20. Kaliaguine, S., Adnot, A., and Lemay, G., *J. Phys. Chem.* **91,** 2886 (1987).
21. Hillebrecht, F. U., Fuggle, J. C., Bennett, P. A., and Zolnierek, *Z. Phys. Rev.* **27**(4), 2179 (1983).
22. Steiner, P., and Hüfner, S., *Solid State Commun.* **44**(4), 559 (1982).
23. Bergeret, G., Gallezot, P., and Imelik, B., *J. Phys. Chem.* **85,** 411 (1981).
24. Tzou, M. S., Kusonoki, M., Asakura, K., Kuroda, H., Moretti, G., and Sachtler, W. M. H., *J. Phys. Chem.* **95,** 5210 (1991).
25. Zhang, Z., Xu, L., and Sachtler, W. M. H., *J. Catal.***131,** 502 (1991).
26. Bhatia, S., Bakhshi, N. N., and Mathews, J. F., *Can. J. Chem. Eng.* **59,** 192 (1981).
27. Elliot, D. J., and Lunsford, J. H., *J. Catal.* **57,** 11 (1979).
28. Vannice, M. A., *J. Catal.* **50,** 228 (1977).
29. Vannice, M. A., *J. Catal.* **37,** 462 (1975).
30. Rieck, J. J., and Bell, A. J., *J. Catal.* **103,** 46 (1987).
31. Thomson, R. T., and Wolf, E. E., *Appl. Catal.* **103,** 46 (1987).
32. Fujimoto, K., Kudo, Y., and Tominga, H., *J. Catal.* **87,** 136 (1984).
33. Bartholomew, C. H., and Barton, W. B., *Am. Chem. Soc., Div. Fuel Chem.* **21**(4), 30 (1976).
34. van Barneveld, W. A. A., and Ponec, V., *J. Catal.* **88,** 382 (1984).
35. Serov, Y. M., Gur'yanova, O. S., Gur'yanova, S. G., and Gryaznov, V. M., *Russ. J. Phys. Chem.* **60**(1), 117 (1986).
36. Gur'yanova, O. S., Serov, Y. M., Gur'yanova, S. G., and Gryaznov, V. M., *Kinet. Catal.* **30**(2), 406 (1989).
37. Augustine, S. M., and Sachtler, W. M. H., *J. Phys. Chem.* **91,** 5953 (1987).
38. Augustine, S. M., Nacheff, M. S., Tsang, C. M., Butt, J. B., and Sachtler, W. M. H., *in* "Proceedings, 10th North American Catal. Soc. Meeting" (J. Ward, Ed.), p. 1. Elsevier, Amsterdam, 1987.
39. Cavalcanti, F. A. P., Stakheev, A. Yu, and Sachtler, W. M. H., *J. Catal.* **134,** 226 (1992).